

Assessment of quantum dot infrared photodetectors for high temperature operation

P. Martyniuk,¹ S. Krishna,^{2,a)} and A. Rogalski¹

¹*Institute of Applied Physics, Military University of Technology, 2 Kaliskiego Str., 00-908 Warsaw, Poland*

²*Center for High Technology Materials, ECE Department, University of New Mexico, 1313 Goddard St SE., Albuquerque, New Mexico 87 106, USA*

(Received 17 April 2008; accepted 6 June 2008; published online 14 August 2008)

Investigation of the performance of quantum dot infrared photodetectors (QDIPs) in comparison to other types of infrared photodetectors operated near room temperature is presented. The model is based on fundamental performance limitations enabling a direct comparison between different infrared material technologies. It is assumed that the performance is due to thermal generation in the active region. Theoretical estimations provide evidence that the QDIP is suitable for noncryogenic operation especially in long-wavelength infrared region, where conventional HgCdTe photodiodes are not viable. Hence it is expected that improvement in technology and design of QDIP detectors will make it useful for practical application. The higher operating speed of QDIP and multispectral capability are considerable advantages in comparison with thermal detectors. Comparison of theoretically predicted and experimental data indicates that, as so far, the QDIP devices have not demonstrated their potential advantages and are expected to possess the fundamental ability to achieve higher detector performance. Poor QDIP performance is generally linked to nonoptimal band structure and control over the QDs size and density. © 2008 American Institute of Physics. [DOI: 10.1063/1.2968128]

I. INTRODUCTION

Since the initial proposal by Esaki and Tsu¹ in 1970 and the advent of molecular beam epitaxy, the interest in semiconductor low-dimensional solids has increased continuously over the years, driven by technological challenges, new physical concepts and phenomena, as well as promising applications. A new class of materials with unique optoelectronic properties has been developed. Zero-dimensional quantum confined semiconductor heterostructures have been investigated theoretically and experimentally for some time.²⁻⁴ At present, nearly defect-free quantum dot (QD) devices can be fabricated reliably and reproducibly. Also new types of infrared photodetectors taking advantage of the quantum confinement obtained in semiconductor heterostructures have emerged. The most advanced III-V infrared detectors, which utilize intersubband or subband-to-continuum transitions in quantum wells, are GaAs/AlGaAs quantum well infrared photodetectors (QWIPs). The imaging performance of focal plane arrays fabricated with this material system can be compared to the state-of-the-art HgCdTe diodes.^{5,6}

The success of quantum well structures for infrared detection applications has stimulated the development of QD infrared photodetectors (QDIPs). In general, QDIPs are similar to QWIPs but with the quantum wells replaced by QDs, which have size confinement in all spatial directions. Recently, Krishna *et al.*⁷ have reviewed progress of QD-based focal plane arrays (FPAs) from the first raster scanned image to a 640 × 512 camera. Also first two-color QDIP camera has

been demonstrated.⁸ One of the main potential advantages of QDIPs is the low dark current. In particular, the lower dark currents enable higher operating temperatures. Until now, however, most of the QDIP devices reported in the literature have been working in the temperature range of 77–200 K. On account of this fact, it is interesting to probe further into achieving a QDIP with performance in the temperature range above 200 K in comparison with other type of detectors.

The objective of this paper is to present a simple set of fundamental IR detector parameters to compare the performance of different material systems (HgCdTe photodiodes, type-II superlattices, and QDs) at near room temperature operation. Our intent is to concentrate on fundamental phenomena and minimize any confusion that might exist. The paper complements two previously published papers by Kinch⁹ and Phillips.¹⁰

II. ANTICIPATED ADVANTAGES OF QDIPS

The quantum-mechanical nature of QDIPs leads to several advantages over QWIPs and other types of IR detectors that are available. As in the HgCdTe, QWIP, and type-II superlattice technologies, QDIPs provide multiwavelength detection. However, QDs provide many additional parameters for tuning the energy spacing between energy levels, such as QD size and shape, strain, and material composition.

The potential advantages in using QDIPs over quantum wells are as follows.

- Intersubband absorption may be allowed at normal incidence (for *n*-type material). In QWIPs, only transitions polarized perpendicularly to the growth direction are allowed due to absorption selection rules. The se-

^{a)}Electronic mail: skrishna@chtm.unm.edu.

lection rules in QDIPs are inherently different, and normal incidence absorption is observed.

- Thermal generation of electrons is significantly reduced due to the energy quantization in all three dimensions. As a result, the electron relaxation time from excited states increases due to phonon bottleneck. Generation by LO phonons is prohibited unless the gap between the discrete energy levels equals exactly to that of the phonon. This prohibition does not apply to quantum wells, since the levels are quantized only in the growth direction and a continuum exists in the other two directions (hence generation/recombination by LO phonons with capture time of few picoseconds). Thus, it is expected that S/N ratio in QDIPs will be significantly larger than that of QWIPs.

- Lower dark current of QDIPs is expected than of HgCdTe detectors and QWIPs due to three-dimensional quantum confinement of the electron wave function.^{11,12}

Both the increased electron lifetime and the reduced dark current indicate that QDIPs should be able to provide high temperature operation. In practice, however, it has been a challenge to meet all of above expectations. Carrier relaxation times in QDs are longer than the typical 1–10 ps measured for quantum wells. It is predicted that the carrier relaxation time in QDs is limited by electron-hole scattering,¹¹ rather than phonon scattering. For QDIPs, the lifetime is expected to be even larger, greater than 1 ns, since the QDIPs are majority carrier devices due to the absence of holes. The main disadvantage of the QDIP is the large inhomogeneous linewidth of the QD ensemble variation of dot size in the Stranski–Krastanow growth mode.^{10,12} As a result, the absorption coefficient is reduced, since it is inversely proportional to the ensemble linewidth. Large, inhomogeneously broadened linewidth has a deleterious effect on QDIP performance. Subsequently, the quantum efficiency of QD devices tend to be lower than what is predicted theoretically. Vertical coupling of QD layers reduces the inhomogeneous linewidth of the QD ensemble; however, it may also increase the dark current of the device, since carriers can tunnel through adjacent dot layers more easily. As in other type of detectors, also nonuniform dopant incorporation adversely affects the performance of the QDIP. Therefore, improving QD uniformity is a key issue in the increasing absorption coefficient and improving the performance. Thus, the growth and design of unique QD heterostructure is one of the most important issues related to achievement of state-of-the-art QDIP performance. However, it must be pointed out that in standard $30 \times 30 \mu\text{m}^2$ pixel, there are about 10^6 QDs (assuming a typical QD density of $1 \times 10^{11} \text{ cm}^{-2}$). Hence the fluctuation from pixel to pixel is not expected to be much larger than that of QWIPs since each pixel samples a large number of QDs.

III. THEORETICAL MODEL FOR QDIP

In further consideration a simple QDIP model developed by Ryzhii *et al.*^{13,14} is adapted. The QDIP consists of a stack of QD layers separated by a wide-gap material layers (see

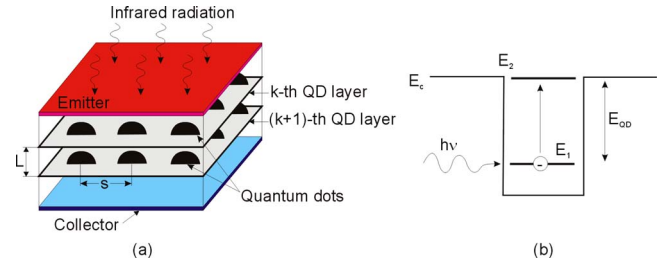


FIG. 1. (Color online) Schematic view of the QD structure (a) and conduction band structure of the dot (b).

Fig. 1). Each QD layer includes periodically distributed identical QDs with the density Σ_{QD} and sheet density of doping donors equal to Σ_D . It is assumed that the lateral size of QDs, a_{QD} , is sufficiently large in comparison with transverse size, l_{QD} . Consequently, a single energy level associated with the quantization in the transverse direction exists. The excited state coincides with the barrier conduction band minimum. Relatively sufficiently large lateral size l_{QD} causes a large number of bound states in dots and, consequently, is capable of accepting large number of electrons. Instead, the transverse size is small in comparison with the spacing between the QD layers, L . The QDIP active region (the stack of QD arrays) is sandwiched between two heavily doped regions which serve as the emitter and collector contacts.

The dark current across the device results from carrier trapping into and thermionic emission from the QDs. The average number of electrons in a QD belonging to the k th QD layer, $\langle N_k \rangle$, can be indicated by a solitary QD layer index ($k=1, 2, \dots, K$, where K is the total number of the QD layers).

A simple algorithm presented in Refs. 13–15 estimates the performance of QDIP such as the dark current, photocurrent, responsivity, and detectivity as a function of the structural parameters.

The average value of current density across the detector active region takes the form

$$\langle j_{\text{dark}} \rangle = q \Sigma_{\text{QD}} \frac{G_{\text{th}}}{p_k}, \quad (1)$$

where

$$G_{\text{th}} = G_o \exp\left(-\frac{E_{\text{QD}}}{kT}\right) \exp\left[\frac{\pi \hbar^2 \langle N_k \rangle}{m^* k T a_{\text{QD}}^2}\right] \quad (2)$$

and

$$p_k = p_{ok} \frac{N_{\text{QD}} - \langle N_k \rangle}{N_{\text{QD}}} \exp\left[-\frac{q^2 \langle N_k \rangle}{C_{\text{QD}} k T}\right]. \quad (3)$$

G_k is the rate of the electron thermoexcitation from QDs, p_k is the capture cross section, G_o is a factor that depends on detector structure, $E_{\text{QD}} = E_2 - E_1$ is the ionization energy of the ground state in QDs, m^* is the effective mass of the electron, \hbar and k are the Planck and Boltzmann constants, respectively, T is the temperature, p_{ok} is the capture probability for uncharged QDs close to 1, N_{QD} is the maximum number of electrons which can occupy each QD, C_{QD} is the QD capacitance given by

$$C_{\text{QD}} \cong \frac{2\varepsilon a_{\text{QD}}}{\pi\sqrt{\pi}}, \quad (4)$$

and ε is the dielectric constant of the material from which the QD is fabricated.

The G_o value provides insight to the physical mechanisms of dark current in QDIPs and is used as a fitting parameter. Assuming decisive contribution of the thermionic emission rate, its value has been estimated as 10^{10} s^{-1} .

In the voltage range $kT \ll qV < q(V_{\text{QD}} - V_D)$, in which QDs are not totally filled, one can obtain

$$\langle N_k \rangle = \frac{V + V_D}{V_{\text{QD}}}. \quad (5)$$

Here, V is the applied voltage, and

$$V_{\text{QD}} = \frac{q}{2\varepsilon_o\varepsilon_r} K(K+1)\Sigma_{\text{QD}}L(1-\vartheta)N_{\text{QD}}, \quad (6)$$

$$V_D = \frac{q}{2\varepsilon_o\varepsilon_r} K(K+1)\Sigma_D L, \quad (7)$$

are the characteristic voltages,

$$\vartheta = \frac{0.72\sqrt{2}}{\pi KL\sqrt{\Sigma_{\text{QD}}}}, \quad (8)$$

and q is the electron charge.

A frequently encountered figure of merit for infrared detector, the R_oA product, can be determined from the relation

$$R_oA = \left(\frac{\partial \langle J_{\text{dark}} \rangle}{\partial V} \right)_{|V_b=0}. \quad (9)$$

It can be shown that

$$R_oA = \frac{\frac{p_{ok}}{qG_o\Sigma_{\text{QD}}} \exp\left[\frac{E_{\text{QD}}}{kT}\right]}{N_{\text{QD}}V_{\text{QD}} \exp\left[\left(\frac{\pi\hbar^2}{m^*kTa_{\text{QD}}^2} + \frac{q^2}{C_{\text{QD}}kT}\right)\frac{V_D}{V_{\text{QD}}}\right]} \times \left[\frac{(N_{\text{QD}}V_{\text{QD}} - V_D)^2}{\left(\frac{\pi\hbar^2}{m^*kTa_{\text{QD}}^2} + \frac{q^2}{C_{\text{QD}}kT}\right)\left(\frac{N_{\text{QD}}V_{\text{QD}} - V_D}{V_{\text{QD}}}\right) + 1} + 1 \right]. \quad (10)$$

The normalized dark current, $J_{\text{dark}} = G_{\text{th}}q$, directly determines thermal detectivity

$$D^* = \frac{\eta}{2hv\sqrt{G_{\text{th}}}}. \quad (11)$$

IV. THEORETICAL MODEL FOR HGCDTE DIODE

Among ten various types of Auger processes, which are possible in InSb-like band structure, two of smallest threshold energy, Augers 1 and 7, are of practical importance in HgCdTe ternary alloy.¹⁶⁻¹⁸ Assuming nondegenerated statistics, the corresponding Auger generation rate is equal to

$$G_A = \frac{n}{2\tau_{A1}^j} + \frac{p}{2\tau_{A7}^j}, \quad (12)$$

where τ_{A1}^j and τ_{A7}^j are the intrinsic Augers 1 and 7 recombination times.

The intrinsic Auger 1 recombination time can be approximated by¹⁹

$$\tau_{A1}^j = 8.3 \times 10^{-13} E_g^{1/2} \left(\frac{q}{kT}\right)^{3/2} \exp\left(\frac{qE_g}{kT}\right), \quad (13)$$

where E_g is in eV.

The ratio of Augers 7 and 1 intrinsic times $\gamma = \tau_{A7}^j / \tau_{A1}^j$ is a term of high uncertainty. According to Ref. 17,

$$\gamma = \frac{\tau_{A7}^j}{\tau_{A1}^j} \approx 2 \frac{m_e^*(E_{\text{th}}) \left(1 - \frac{5E_{\text{th}}}{4kT}\right)}{m_{\text{eo}}^* \left(1 - \frac{3E_{\text{th}}}{2kT}\right)}. \quad (14)$$

For the Auger 7 process the threshold energy $E_{\text{th}} \approx E_g$. From Kane's nonparabolic approximation $m_e^*(E_{\text{th}})/m_{\text{eo}}^* \approx 3$, and for $\text{Hg}_{1-x}\text{Cd}_x\text{Te}$ over the ranges of $0.16 \leq x \leq 0.40$ and $50 \leq T \leq 300 \text{ K}$, $3 \leq \gamma \leq 6$. As the γ is higher than unity, a higher recombination lifetimes are expected in lightly doped p -type materials.

The Auger dominated detectivity can be determined using²⁰

$$D^* = \frac{\lambda}{2hc} \frac{\eta}{t^{1/2}} G_A^{-1/2} = \frac{\lambda}{2^{1/2}hc} \frac{\eta}{t^{1/2}} \left(\frac{\tau_{A1}^j}{n + \frac{p}{\gamma}} \right)^{1/2}. \quad (15)$$

The detectivity is proportional to the factor $\eta/t^{1/2}$, and then high quantum efficiency must be achieved in thin devices.

Since the resulting Auger generation rate achieves its minimum for $p = \gamma^{1/2}n_i$, it leads to important conclusion about optimum doping. The optimum performance of Auger limited HgCdTe detectors can be achieved with a lightly p -type doping with hole concentration $p = \gamma^{1/2}n_i$. The required p -type doping is difficult to achieve in practice for low temperature photodiodes, and the p -type material suffers from some nonfundamental limitations, such as contacts, surface, and Shockley-Read processes. These are the reasons why the low temperature detectors are typically produced from the lightly doped n -type materials. However, the p -type doping is clearly advantageous for near room temperature HgCdTe detectors.

The thickness of the detector's base region should be optimized to receive near unity quantum efficiency and a low dark current. This is achieved using the base layer thickness comparable to the inverse absorption coefficient $t = 1/\alpha$. In this context a choice of the p -type base layer is more motivated due to a little higher absorption coefficient in comparison with n -type material.

For an ideal diffusion-limited diode $J_D = J_s [\exp(qV/kT) - 1]$. Assuming that the saturation dark current density J_s of a photodiode is only due to thermal generation in the base layer and that its thickness is low compared to the diffusion length, we have

$$J_s = qG_{th}t, \quad (16)$$

where G_{th} is the thermal generation rate in the base layer. Because the zero bias resistance-area product is

$$R_oA = \frac{kT}{qJ_s}, \quad (17)$$

so

$$R_oA = \frac{kT}{q^2G_{th}t}. \quad (18)$$

Taking into account the Auger 7 mechanism in extrinsic p -type region of n -on- p photodiode, we obtain

$$R_oA = \frac{2kT\tau_{A7}^j}{q^2N_d t}, \quad (19)$$

and the same equation for p -on- n photodiode

$$R_oA = \frac{2kT\tau_{A1}^j}{q^2N_d t}, \quad (20)$$

where N_a and N_d are the acceptor and donor concentrations in the base regions, respectively.

V. COMPARISON OF QDIPS AND HgCdTe DEVICES

Most modern infrared FPAs are fabricated from two pieces of material—a detector array made from compound semiconductor materials and a silicon signal processing chip called a readout integrated circuit (ROIC). The ROIC amplifies the signal from each detector element and performs processing functions by multiplexing the signals of thousands of pixels onto a few output lines. The infrared arrays have individual-amplifier-per-detector readouts based on metal oxide semiconductor field effect transistors (MOSFETs). The operating point of the coupled detector and input circuit is found by constructing a load line for the I - V characteristics of the detector and input MOSFET. The input impedance of a MOSFET is a function of the source-drain current (in this case, the total diode current) and is usually expressed in terms of the transconductance g_m given by $qI/(nkT)$ for low injected currents (n is an ideality factor that can vary with temperature and geometry of the transistor and usually is in the range of 1–2).

The injection efficiency is approximately given by^{21,22} (is this only true for direct injection ROIC?)

$$\varepsilon = \frac{IR_d}{IR_d + (nkT/q)}, \quad (21)$$

where R_d is the dynamic impedance of the detector and I is the total injected detector current (the sum of the photocurrent and the dark current) equal photocurrent I_{ph} in the background-limited case.

To receive high injection efficiency, the input impedance of the MOSFET must be much lower than the internal dynamic resistance of the detector at its operating point, and the following condition should be fulfilled:²³

$$IR_d \gg \frac{nkT}{q}. \quad (22)$$

TABLE I. Material parameters of QDs in QDIP calculations.

a_{QD}	Σ_{QD}	Σ_D	L	K	N_{QD}	ε_r	m^*/m
15 nm	10^{11} cm^{-2}	$6 \times 10^{10} \text{ cm}^{-2}$	100 nm	10	6	12	0.023

For most applications, the detector performance depends on operating the detector in a small bias where the dynamic resistance is at a maximum. It is then necessary to minimize extraneous leakage current. The control of these leakage currents and the associated low-frequency noise is therefore of crucial interest.

A. Dark current and R_oA product

Generally, it is not problem to fulfil inequality (22) for short wavelength infrared and middle wavelength infrared (MWIR) FPAs where the dynamic resistance of detector R_d is large, but it is very important for LWIR designs where R_d is low. There are more complex injection circuits that effectively reduce the input impedance and allow lower detector resistance to be used.

The above requirement is especially critical for near room temperature HgCdTe photodetectors operating in LWIR region. Their resistance is very low due to a high thermal generation. In materials with a high electron to hole ratio as HgCdTe, the resistance is additionally reduced by ambipolar effects. Small size uncooled $10.6 \mu\text{m}$ photodiodes ($50 \times 50 \mu\text{m}^2$) exhibit less than 1Ω zero bias junction resistances which are well below the series resistance of a diode. As a result, the performance of conventional devices is very poor, so they are not usable for practical applications. To fulfil inequality (22) to effectively couple the detector with silicon readout, the detector incremental resistance should be $R_d \gg 2 \Omega$.

Material parameters that are used for QDIP calculations are listed in Table I. They are representative of self-assembled InAs/GaAs QDs reported in the literature.^{10,12–15} The dependence of the material parameters of $\text{Hg}_{1-x}\text{Cd}_x\text{Te}$ on composition x , necessary in calculations, has been determined according to Ref. 20. Figure 2 presents the dark current density of HgCdTe photodiodes and QDIPs as a function of cutoff wavelength at 200, 250, and 300 K. As Fig. 2

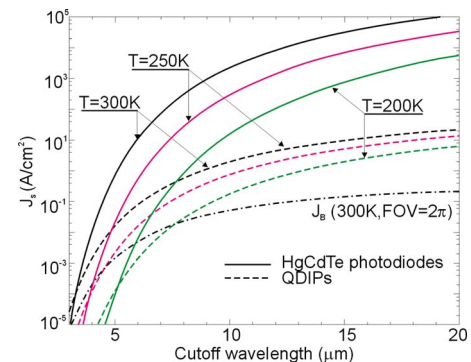


FIG. 2. (Color online) Dark current density of HgCdTe photodiodes and QDIPs and background-generated photocurrent as a function of wavelength. The calculations for HgCdTe photodiodes have been performed for the optimized doping concentration $p = \gamma^{1/2}n_i$.

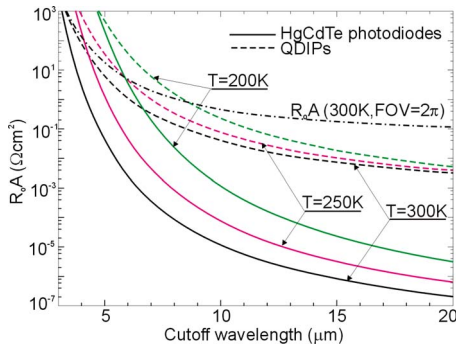


FIG. 3. (Color online) $R_o A$ product of HgCdTe photodiodes and QDIPs as a function of wavelength. The calculations for HgCdTe photodiodes have been performed for the optimized doping concentration $p = \gamma^{1/2} n_i$.

shows, the saturation current of 10 μm HgCdTe photodiode achieves 1000 A/cm^2 and it is by four orders of magnitude larger than the photocurrent due to the 300 K background radiation. The potential advantages of QDIPs are considerably lower dark current and higher $R_o A$ product in comparison with HgCdTe photodiodes (see Fig. 3).

B. Detectivity

Figure 4 compares the calculated thermal detectivity of HgCdTe photodiodes and QDIPs as a function of wavelength and operating temperature with the experimental data of near room temperature HgCdTe and type-II InAs/GaInSb strained layer superlattice (SLS) detectors. The calculations for HgCdTe photodiodes have been performed for optimized

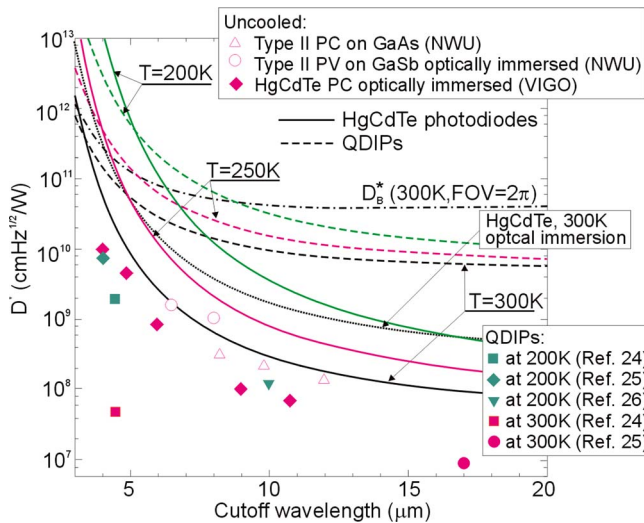


FIG. 4. (Color online) Calculated performance of Auger generation-recombination limited HgCdTe photodetectors as a function of wavelength and operating temperature. Background limited detectivity has been calculated for 2π FOV, the background temperature is $T_{\text{BLIP}}=300$ K, and the quantum efficiency $\eta=1$. The calculations for HgCdTe photodiodes have been performed for the optimized doping concentration $p = \gamma^{1/2} n_i$. The experimental data are taken for commercially available uncooled HgCdTe photoconductors (produced by Vigo System) and uncooled type-II detectors at the Center for Quantum Devices, Northwestern University (after <http://cqcd.northwestern.edu/research/type2.php>). The experimental data for QDIPs are gathered from the marked literature for detectors operated at 200 and 300 K.

doping concentration $p = \gamma^{1/2} n_i$. The experimental data for QDIPs are gathered from the literature for detectors operated at 200 and 300 K.^{24–26}

Uncooled LWIR HgCdTe photodetectors are commercially available and manufactured in significant quantities, mostly as single-element devices.^{27–29} They have found important applications in IR systems that require fast response. The results presented in Fig. 4 confirm that the type-II superlattice is a good candidate for IR detectors operating in the spectral range from the midwavelength to the very long-wavelength IR. However, comparison of QDIP performance both with HgCdTe and type-II superlattice detectors gives clear evidence that the QDIP is suitable for high temperature operation. Especially encouraging results have been achieved for very long-wavelength QDIP devices with a double-barrier resonant tunneling filter with each QD layer in the absorption region.^{30,31} In this type of devices, photoelectrons are selectively collected from the QDs by resonant tunneling, while the same tunnel barriers block electrons of dark current due to their broad energy distribution. For the 17 μm detector, a peak detectivity of 8.5×10^6 $\text{cm Hz}^{1/2}/\text{W}$ has been measured. Up until now, this novel device demonstrates the highest performance of room temperature photodetectors. Further improvement in technology and design can result in application of QDIPs in room temperature focal plane arrays with the advantages of larger operating speed (shorter frame time) in comparison with thermal detectors (bolometers and pyroelectric devices).

The room temperature operation of thermal detectors makes them lightweight, rugged, reliable, and convenient to use. However, their performance is modest, and they suffer from slow response. Because they are nonselective detectors, their imaging systems contain very broadband optics, which provide impressive sensitivity at a short range in good atmospheres. Thermal detectors seem to be unsuitable for the next generation of IR thermal imaging systems, which are moving toward faster frame rates and multispectral operation. A response time much shorter than that achievable with thermal detectors is required for many nonimaging applications. Improvements in technology and design of QDIP detectors make it possible to achieve both high sensitivity and fast response at room temperature.

VI. SUMMARY AND CONCLUSIONS

The intent of this paper is to compare the achievements of QDIP technology in near room temperature operation with those of competitive technologies, with the emphasis on the material properties, device structure, and their impact on the device performance, especially in LWIR spectral regions.

At present, HgCdTe is the most widely used variable-gap semiconductor that has a privileged position both in the MWIR as well as LWIR spectral ranges. Theoretical predictions indicate that type-II superlattice photodiodes and QDIPs are expected to compete with HgCdTe photodiodes.³² However, the measured values of QDIPs' detectivities at temperature of 77 K are considerably inferior to current HgCdTe detector performance.

Theoretical estimations carried out in this paper give

clear evidence that the QDIP is suitable for high operation temperature. Especially encouraging results have been recently achieved for very long-wavelength QDIP devices with a double-barrier resonant tunneling filter. Due to the fact that conventional HgCdTe photodiodes are not usable for room temperature FPA applications, it can be expected that improvement in technology and design of QDIP detectors will make it possible to achieve both high sensitivity and fast response useful for practical application in room temperature FPAs. This new generation of room temperature FPAs will eventually compete with silicon microbolometers dominant at present. Larger operating speed of QDIP and multispectral capability are considerable advantages in comparison with thermal detectors.

Improving QD uniformity is a key issue in increasing the absorption coefficient and improving the performance. Optimization of the QDIP architecture is still an open area. Since some of the design parameters depend on a device structure (photoconductive and noise gains, dark current, quantum efficiency), the performance is still being improved.

ACKNOWLEDGMENTS

This work was supported by funding from AFRL/NSF. Support from Gladden Fellowship is acknowledged.

¹L. Esaki and R. Tsu, *IBM J. Res. Dev.* **14**, 61 (1970).

²Y. Arakawa and H. Sakaki, *Appl. Phys. Lett.* **40**, 939 (1982).

³M. Asada, Y. Miyamoto, and Y. Suematsu, *IEEE J. Quantum Electron.* **QE-22**, 1915 (1986).

⁴D. Bimberg, M. Grundmann, and N. N. Ledentsov, *Quantum Dot Heterostructures* (Wiley, Chichester, 1999).

⁵S. D. Gunapala and S. V. Bandara, in *Handbook of Infrared Detection Technologies*, edited by M. Henini and M. Razeghi (Elsevier, Oxford, 2002), pp. 83–119.

⁶A. Rogalski, *J. Appl. Phys.* **93**, 4355 (2003).

⁷S. Krishna, S. D. Gunapala, S. V. Bandara, C. Hill, and D. Z. Ting, *Proc. IEEE* **95**, 1838 (2007).

⁸E. Varley, M. Lenz, S. J. Lee, J. S. Brown, D. A. Ramirez, A. Stintz, and S. Krishna, *Appl. Phys. Lett.* **91**, 081120 (2007).

⁹M. A. Kinch, *J. Electron. Mater.* **29**, 809 (2000).

¹⁰J. Phillips, *J. Appl. Phys.* **91**, 4590 (2002).

¹¹I. Vurgaftman, Y. Lam, and J. Singh, *Phys. Rev. B* **50**, 14309 (1994).

¹²E. Towe and D. Pan, *IEEE J. Sel. Top. Quantum Electron.* **6**, 408 (2000).

¹³V. Ryzhii, I. Khmyrova, V. Pipa, V. Mitin, and M. Willander, *Semicond. Sci. Technol.* **16**, 331 (2001).

¹⁴V. Ryzhii, I. Khmyrova, V. Mitin, M. Stroschio, and M. Willander, *Appl. Phys. Lett.* **78**, 3523 (2001).

¹⁵V. Ryzhii, *Jpn. J. Appl. Phys., Part 2* **40**, L148 (2001).

¹⁶P. E. Petersen, in *Semiconductors and Semimetals Vol. 18*, edited by R. K. Willardson and A. C. Beer (Academic, New York, 1981), pp. 121–155.

¹⁷T. N. Casselman and P. E. Petersen, *Solid State Commun.* **33**, 615 (1980).

¹⁸T. N. Casselman, *J. Appl. Phys.* **52**, 848 (1981).

¹⁹M. A. Kinch, M. J. Brau, and A. Simmons, *J. Appl. Phys.* **44**, 1649 (1973).

²⁰A. Rogalski and R. Ciupa, *J. Appl. Phys.* **77**, 3505 (1995).

²¹P. Felix, M. Moulin, B. Munier, J. Portmann, and J.-P. Reboul, *IEEE Trans. Electron Devices* **ED-27**, 175 (1980).

²²V. Gopal, *Opt. Eng.* **33**, 809 (1994).

²³J. L. Vampola, in *The Infrared and Electro-Optical Systems Handbook*, edited by W. D. Rogatto (SPIE Optical Engineering, Bellingham, 1993), Vol. 3, pp. 285–342.

²⁴H. Lim, S. Tsao, W. Zhang, and M. Razeghi, *Appl. Phys. Lett.* **90**, 131112 (2007).

²⁵S. Chakrabarti, A. D. Stiff-Roberts, X. H. Su, P. Bhattacharya, G. Ariyawansa, and A. G. U. Perera, *J. Phys. D* **38**, 2135 (2005).

²⁶X. Lu, J. Vaillancourt, and M. J. Meisner, *Appl. Phys. Lett.* **91**, 051115 (2007).

²⁷J. Piotrowski and A. Rogalski, *Infrared Phys. Technol.* **46**, 115 (2004).

²⁸Vigo System, www.vigo.com.pl

²⁹J. Piotrowski and A. Rogalski, *High-Operating Temperature Infrared Photodetectors* (SPIE, Bellingham, 2007).

³⁰X. H. Su, S. Chakrabarti, P. Bhattacharya, A. Ariyawansa, and A. G. U. Perera, *IEEE J. Quantum Electron.* **41**, 974 (2005).

³¹A. G. U. Perera, G. Ariyawansa, V. M. Apalkov, S. G. Matsik, X. H. Su, S. Chakrabarti, and P. Bhattacharya, *Opto-Electron. Rev.* **15**, 223 (2007).

³²P. Martyniuk and A. Rogalski, *Proc. SPIE* **6940**, 6940 (2008).